Dynamical Downscaling of the Climate for the Hawaiian Islands. Part II: Projection for the Late Twenty-First Century

CHUNXI ZHANG, YUQING WANG, KEVIN HAMILTON, AND AXEL LAUER[a]

International Pacific Research Center, and Department of Atmospheric Sciences, School of Ocean and Earth Science and Technology, University of Hawai'i at Mānoa, Honolulu, Hawaii

(Manuscript received 31 December 2015, in final form 8 June 2016)

ABSTRACT

A 20-yr simulation with a fine-resolution regional atmospheric model for projected late twenty-first-century conditions in Hawaii is presented. The pseudo-global-warming method is employed, and the boundary conditions are based on a multimodel mean of projections made with global coupled models run with a moderate greenhouse gas emissions scenario. Results show that surface air temperature over land increases ~2°–4°C with the greatest warming at the highest topographic heights. A modest tendency for the warming to be larger on the leeward sides of the major islands is also apparent. Climatological rainfall is projected to change up to ~25% at many locations. The currently wet windward sides of the major islands will have more clouds and receive more rainfall, while the currently dry leeward sides will generally have even less clouds and rainfall. The average trade wind inversion–base height and the mean marine boundary layer cloud heights are projected to exhibit only small changes. However, the frequency of days with clearly defined trade wind inversions is predicted to increase substantially (~83% to ~91%). The extreme rainfall events are projected to increase significantly. An analysis of the model's moisture budget in the lower troposphere shows that the increased mean rainfall on the windward sides of the islands is largely attributable to increased boundary layer moisture in the warmer climate. Rainfall changes attributable to mean low-level circulation changes are modest in comparison.

1. Introduction

The seven regularly inhabited islands in the U.S. state of Hawaii are home to over 1.4 million full-time residents as well as a large transient population of visitors. While Hawaii is renowned for its generally pleasant weather, anticipated climate change over the present century will likely present significant challenges for its inhabitants. Sea level rise and a warming ocean surface, with consequent effects on beach erosion and coral health, are familiar issues for Hawaii (e.g., Jokiel and Brown 2004; Romine et al. 2013). However, there are also significant concerns directly related to changes in prevailing weather conditions, including possible effects of changing rainfall and evapotranspiration on freshwater resources as well as impacts of atmospheric and surface warming on plant and wildlife habitat. Leong et al. (2014) reviewed current research on climate change vulnerabilities in Hawaii. Here we will briefly discuss some of the key issues motivating our own climate projection work.

As on most isolated islands, the reliable supply of freshwater is a potentially serious concern in Hawaii. Even under present conditions wildfires occurring during dry conditions represent a significant problem on all the major Hawaiian Islands (Trauernicht et al. 2015). Available surface and groundwater resources are scarce enough that water use restrictions are common in some areas during droughts, while agricultural demands for groundwater have sparked a history of public controversy and litigation on at least one of the islands (Maui). According to King (2014) "agriculture in Central Maui currently operates at a water deficit with today's average rainfall pattern.... There is the distinct possibility that Hawaii rainfall will decrease in the future. More drought-tolerant and less water-hungry crops will be needed."

A climate change issue of special concern in Hawaii, and one with implications beyond Hawaii's own population, is the likely impact on biodiversity. Despite its

[a] Current affiliation: Deutsches Zentrum für Luft- und Raumfahrt (DLR), Institut für Physik der Atmosphäre, Oberpfaffenhofen, Germany.

Corresponding author address: Dr. Yuqing Wang, IPRC/SOEST, POST Bldg., Room 404A, 1680 East-West Road, Honolulu, HI 96822. E-mail: yuqing@hawaii.edu

DOI: 10.1175/JCLI-D-16-0038.1

small land area, Hawaii stands out globally as a ''hot spot'' of terrestrial biodiversity. There are more than 1000 species of flora and 100 species of birds endemic to (i.e., naturally found only in) Hawaii (James 1995; Sakai et al. 2002; Duffy and Kraus 2006). Unfortunately Hawaii is also a notable center for species extinction and endangerment. According to Duffy and Kraus (2006), ''of the 107 endemic bird species present before the arrival of humans around 400 A.D., only 10 percent are either not extinct or not threatened with extinction. . . . Almost 300 plant species, or about 30 percent of the endemic native flora, are threatened or endangered, and a similar number are in decline.'' While the state of Hawaii has only about 1/500 of the total landmass of the United States, well over one-quarter of the plant and bird species on the U.S. government's official endangered list are found only in Hawaii. In a classic study Benning et al. (2002) conclude that ''anthropogenic climate change is likely to combine with past land use changes and biological invasions to drive several of the remaining species [of birds] to extinction, especially on the islands of Kauai and Hawaii.'' Krushelnycky et al. (2013) studied the effects of recent climate change on the charismatic flowering bush known as the Haleakala silversword (*Argyroxyphium sandwicense*) and concluded ''. . . this iconic species has entered a period of substantial climate-associated decline,'' a trend that can be expected to lead to a ''bleak future'' if prevailing conditions at high altitudes continue to become warmer and drier. Krushelnycky et al. (2013) go on to state, ''the silversword example . . . illustrates how even well-protected and relatively abundant species may succumb to climate-induced stresses.''

While published research on climate-related stress has concentrated on a limited number of species, it is likely that climate change in Hawaii will threaten many species and perturb terrestrial and coastal ecosystems, with unfortunate effects on the state's remarkable contribution to global biodiversity. Another wide-ranging concern is the influence of climate change on terrestrial primary productivity and carbon storage in Hawaii (Bothwell et al. 2014), effects that contribute to the global biogeochemical feedbacks that regulate global climate. Hawaii has been proposed as a site for major biofuel crop production, with global implications for possible greenhouse gas mitigation strategies (Tran et al. 2011).

The challenges of adaptation to climate change have a high public profile in Hawaii. An eloquent summary of the public and political view is provided by this excerpt from recent legislation: ''Climate changes will likely impose major, but not fully understood, costs and other impacts on Hawaii's people and the natural capital we depend upon to support our lives in the middle of the Pacific Ocean. Nowhere is it more obvious than in remote island chains like Hawaii that our lives and the economy are intertwined with the health and function of the natural world around us. . . . Now is the time . . . [to] plan for and address the inevitable effects of climate change'' [Food and Energy Security, Act 73, Hawaii H.B. 2421, 25th Leg., preamble (2010)].

While the need for reliable Hawaii climate projections to guide policymakers and other stakeholders is widely appreciated, only quite limited research on future climate in Hawaii has been published. Little directly applicable information about Hawaii climate change is provided by the reports of the Intergovernmental Panel on Climate Change (IPCC). Some investigators have used statistical methods to downscale projected rainfall changes (Elison Timm and Diaz 2009; Norton et al. 2011; Elison Timm et al. 2013, 2015). Major national efforts to dynamically downscale the projected climate changes from the Climate Model Intercomparison Project (CMIP) global models over North America have not included Hawaii, and in any event the horizontal resolution of the regional models employed have been much too coarse for useful application to Hawaii (Mearns et al. 2012; http://nrmsc.usgs.gov/RegClimateDownscaling).

The major islands of Hawaii are notable for the presence of very fine-structure microclimates (e.g., Lyons 1982; Chu et al. 1993; Schroeder 1993; Esteban and Chen 2008; Giambelluca et al. 2013, 2014; Zhang et al. 2016), and this represents a particular challenge in bridging the gap between global model outputs with horizontal resolution ~100 km and the needs of stakeholders for quite local information. Zhang et al. (2016), Part I of the present two-part study, have shown results from a nested grid regional atmospheric model with 3-km horizontal resolution over the main Hawaiian Islands and the surrounding ocean region. They showed that their model can simulate the current mean climate of the islands reasonably well but that deficiencies in the simulated mean rainfall distribution are still apparent, particularly in Maui, Oahu, and Kauai. Zhang et al. (2016) speculated that the problems with the rainfall simulation may be related to insufficient horizontal resolution of the topography even at 3-km grid spacing. They performed a simulation with a 1-km-resolution domain for Maui and the adjacent ocean nested within the 3-km Hawaii regional domain and demonstrated a substantial improvement in the rainfall simulation. The results of Zhang et al. (2016) suggest that a numerical model can adequately represent the microclimates on Hawaii (hereinafter referred to as the Big Island) with ~3-km resolution but that for Maui, Oahu, and Kauai (all featuring steeper typical topographic slopes than the

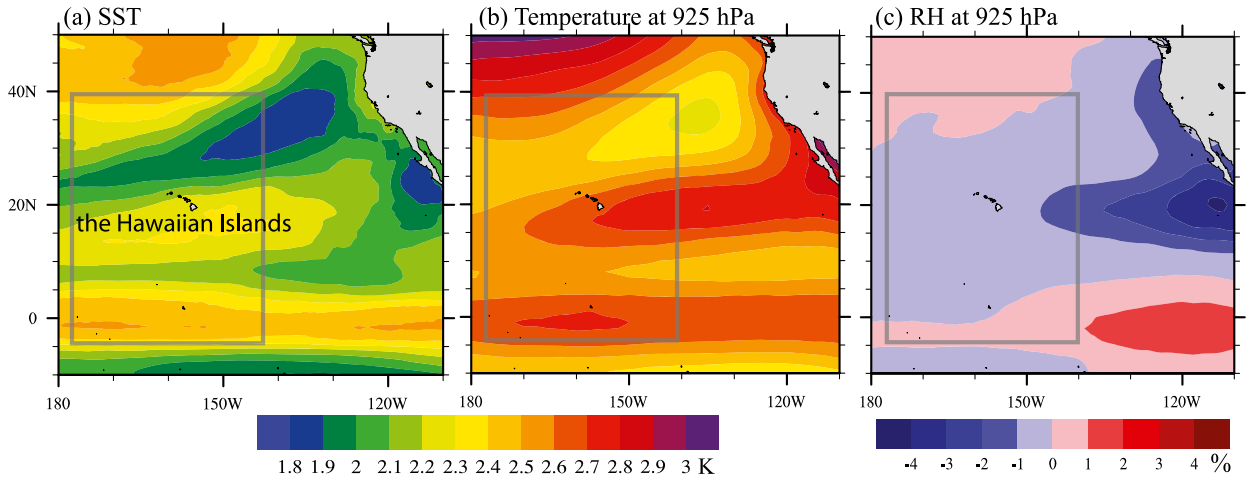

FIG. 1. Annual mean values of the warming increments computed from the CMIP3 multimodel ensemble for the SRES A1B scenario and applied at the boundaries of the late twenty-first-century simulation. The box shows domain 1 of the HRCM.

Big Island) finer resolution can significantly improve results in many localities.

The results of Zhang et al. (2016) encouraged us to apply the same model to downscale future climate projections based on global model results. The present paper reports on this work, including projections at 1-km horizontal resolution for Maui. The simulations we performed are computationally demanding, and this limited the length of integrations, the number of ensemble members, and the variety of scenarios that could be explored. The approach adopted was aimed at providing stakeholders with the best possible practical guidance concerning projected changes in mean climate. Our work serves as well as a pioneering demonstration of very high-resolution dynamical downscaling of climate projections [see Prein et al. (2015) for a summary of current efforts in this area of research]. More details will be provided in section 2 below, but briefly, we conducted a single 20-yr "time slice" simulation meant to be representative of late twenty-first-century conditions, which can be compared with the Zhang et al. (2016) retrospective simulation for 1990–2009. The anticipated effects of changing climate forcing from increasing long-lived greenhouse gas concentrations were introduced into our model using the so-called pseudo-global-warming (PGW) method (Kimura and Kitoh 2007; Sato et al. 2007; Knutson et al. 2008; Hara et al. 2008; Kawase et al. 2009). In the PGW approach, initial and boundary conditions are given by the sum of observed values (atmospheric reanalysis data and observed SSTs) and a climate perturbation signal [global warming increment (GWI)]. The global warming increments were computed from publicly available simulations with global coupled ocean–atmosphere models. The limitations of the PGW approach and other details of our model experiment are discussed in section 2 below.

The rest of the paper is organized as follows. Section 2 briefly reviews the model configuration and then describes the global warming experiment as well as providing some background on the local climate in Hawaii. Section 3 presents the results from the warming experiment. Section 4 is a further discussion of the results and a summary of our main conclusions.

2. Model and methods

a. *Regional model and present-day simulation*

The Hawaiian regional climate model (HRCM), which is based on the Weather Research and Forecasting (WRF) Model, version 3.3.1, is described by Zhang et al. (2012a, 2016) and Lauer et al. (2013). The HRCM is derived from WRF version 3.3.1 by making changes in convective and microphysics parameterizations and by including a detailed specification of the land surface properties for the Hawaiian Islands. For the present study the model is configured with one-way nesting of three meshes. The outer mesh covers a ~4000 km × 5000 km region (see Fig. 1) with 15-km grid spacing, the intermediate mesh has 3-km resolution over a ~800 km × 600 km region covering the main Hawaiian Islands and surrounding ocean, and the innermost mesh has 1-km resolution and covers the island of Maui and the adjacent ocean region.

The "present day" retrospective HRCM integration described in Zhang et al. (2016) is for the period 1990–2009. The sea surface temperatures (SSTs) were specified from the Reynolds et al. (2007) daily analysis, and the lateral boundary conditions were taken from the NASA Modern-Era Retrospective Analysis for Research

and Applications (MERRA; Rienecker et al. 2011). Zhang et al. (2016) assessed how well the model reproduces various aspects of the observed climate during 1990–2009. A key result is that the model simulates the typical vertical sounding with a well-mixed marine boundary layer capped by a trade wind inversion (TWI) layer at heights ranging from 1000 to 4000 m above sea level (Cao et al. 2007). Observations suggest that about 80% of atmospheric soundings in Hawaii have well-defined TWIs, and the HRCM captures this well. The HRCM does display a low bias of about 100 m in the mean TWI base height. Zhang et al. (2016) also show that the 3-km resolution HRCM successfully simulates the broad features of the geographical and seasonal distributions of rainfall on the islands. Notably, the strong gradients between heavy mean rainfall over the windward sides of the islands and the pronounced rain shadow over the leeward areas are reproduced in the simulation. Zhang et al. (2016) speculated that remaining deficiencies in the simulation of the geographical distribution of climatological rainfall in Kauai, Maui, and Oahu may be attributed to inadequate resolution of the very high and steep topography on these islands. Zhang et al. (2016) show that the simulation over Maui in the 1-km-resolution inner mesh does indeed produce an improved simulation of the mean rainfall distribution.

b. *Future simulation*

In this project we complemented the 1990–2009 retrospective simulation of Zhang et al. (2016) with a HRCM simulation meant to represent conditions in 2080–99, assuming the global atmospheric composition evolves as in the A1B scenario of the Special Report on Emissions Scenarios (SRES; IPCC 2000). The A1B scenario assumes rapid growth in the global economy and increasing greenhouse gas emissions through the first half of this century with some moderation starting around midcentury; it has been adopted in many studies as a ''middle of the road'' and quite plausible scenario with which to examine model projections of the twenty-first century climate change. The long-lived greenhouse gas concentrations in the model runs are prescribed using the A1B option in the WRF radiation code. Over the 20-yr period 1990–2009 the prescribed carbon dioxide concentration increases gradually from about 360 to 390 ppmv and during 2081–2100 from about 660 to 720 ppmv. The prescribed methane and nitrous oxide concentrations also increase and chlorofluorocarbon concentrations decrease according to the A1B scenario.

Our goal was to downscale projections of climate change made with global coupled ocean–atmosphere models, and so we based our lateral and ocean surface boundary conditions applied to the HRCM in the 2080–99 simulation on global model simulations that were also forced with the A1B emissions scenario. We employed the PGW method (Sato et al. 2007; Kimura and Kitoh 2007; Knutson et al. 2008; Kawase et al. 2009; Lauer et al. 2013). In the PGW method, initial and boundary conditions for the regional model integrations are updated continuously and are given by the sum of observations (observed gridded SSTs and atmospheric reanalysis data) and a perturbation we call the global warming increment, which is meant to account for the large-scale forced climate response to enhanced greenhouse gas concentrations.

The GWIs are a function of location, altitude, and calendar date and were computed as the averaged global model simulated 2080–99 results minus the 1990–2009 values. The monthly mean GWIs are interpolated linearly in time before being added to the 6-hourly reanalysis data used to create the lateral boundary conditions or daily SST data to create ocean surface boundary conditions for HRCM. We used results from 20 CMIP3 models (Table 1) that provided all data needed for specifying the climate change contribution to the boundary conditions in HRCM. This includes data from 1) the twentieth-century forced runs (20C3M) and 2) from the late twenty-first century in the SRES A1B runs. If there are multiple ensemble members available for any given model, we consider only one, as the differences in the mean warming signals among the individual models are generally larger than those among individual ensemble members from the same model. The annual mean of the GWI of SST, air temperature at 925 hPa, and relative humidity (RH) at 925 hPa are illustrated in Figs. 1a, 1b, and 1c, respectively. The multimodel mean increment for SST near Hawaii is about 2.1–2.3 K, while the corresponding air temperature increment at 925 hPa is ~2.5–2.7 K. The RH increment is quite small (reduction of less than 1%). The soil moisture and temperature are initialized with the European Centre for Medium-Range Weather Forecasts (ECMWF) interim reanalysis (ERA-Interim) data (Dee et al. 2011). The specified land surface parameters (snow-free albedo, land-use type, green vegetation fraction, and vegetation type) were taken to be the same as those used in the present-day simulations.

We adopted the PGW approach rather than a more straightforward dynamical downscaling applied directly to present-day and future scenario integrations with an individual global model. State-of-the-art global coupled models when run freely generally display large biases in simulated mean SST (magnitudes as large as ~2 K or more in many locations; e.g., Ashfaq et al. 2011; Zheng et al. 2011; Flato et al. 2013) and other variables

TABLE 1. The CMIP3 models used for the ensemble mean GWI. Expansions of institutions and model names are available online at http://www.ametsoc.org/PubsAcronymList.

Originating group(s)	Country	CMIP3 ID
Bjerknes Centre for Climate Research	Norway	BCCR-BCM2.0
National Center for Atmospheric Research	United States	CCSM3
Météo-France/Centre National de Recherches Météorologiques	France	CNRM-CM3
CSIRO Atmospheric Research	Australia	CSIRO Mk3.0
CSIRO Atmospheric Research	Australia	CSIRO Mk3.5
U.S. Dept. of Commerce/NOAA/Geophysical Fluid Dynamics Laboratory	United States	GFDL CM2.0
U.S. Dept. of Commerce/NOAA/Geophysical Fluid Dynamics Laboratory	United States	GFDL CM2.1
LASG/Institute of Atmospheric Physics	China	FGOALS-g1.0
Instituto Nazionale di Geofisica e Vulcanologia	Italy	INGV-SXG
Institute for Numerical Mathematics	Russia	INM-CM3.0
L'Institut Pierre-Simon Laplace	France	IPSL-CM4
Center for Climate System Research (The University of Tokyo), National Institute for Environmental Studies, and Frontier Research Center for Global Change (JAMSTEC)	Japan	MIROC3.2 (hires)
Max Planck Institute for Meteorology	Germany	ECHAM5/MPI-OM
Meteorological Research Institute	Japan	MRI-CGCM2.3.2
Canadian Centre for Climate Modelling and Analysis	Canada	CGCM3.1 (T63)
National Center for Atmospheric Research	United States	PCM
Met Office Hadley Centre	United Kingdom	HadCM3
Met Office Hadley Centre	United Kingdom	HadGEM1
NASA Goddard Institute for Space Studies	United States	GISS-EH
NASA Goddard Institute for Space Studies	United States	GISS-ER

(e.g., Lauer and Hamilton 2013). Such biases may matter significantly for future projections (Sato et al. 2007; Ashfaq et al. 2011). By using observed SSTs and lateral boundary conditions the PGW approach allows one to avoid potentially serious errors in reproducing the observed present-day climate (Kimura and Kitoh 2007). The other major advantage of the PGW approach is that it allows the large-scale forcing of the model to be based on a multimodel ensemble mean GWI. Lauer et al. (2013) conducted downscaling experiments with the outermost mesh of the HRCM using GWIs from 10 individual global models and compared the results with those from experiments using the multimodel mean GWI. Lauer et al. (2013) showed that despite a fairly large intermodel spread in the simulated climate changes, a single downscaling experiment using a multimodel mean GWI gives quite similar results to the ensemble mean of downscaling experiments using warming increments obtained from each of the individual global models.

Of course, the PGW method has important limitations that should be kept in mind when interpreting the downscaling results presented in the next section. Most notably, the PGW method cannot adequately account for possible global-warming-induced changes in the variability of the climate system (from daily to interannual time scales). The PGW method simply imposes the same temporal variability in the boundary conditions in the present day and in the future climate runs. A more direct approach would allow us to downscale global model projections of the change of variability as well as the change in mean climate. Many global model studies have been devoted to projecting the changes in interannual variability forced by increasing greenhouse gas concentrations. However, there remains great uncertainty in such projections even about basic issues as whether El Niño–related variability will intensify or weaken in a warmer climate (e.g., Collins et al. 2010). The issue is quite subtle as characterization of the interannual variability itself from only a century or less of model realization may be inadequate (Wittenberg 2009). Stevenson et al. (2012) examined results from ensembles of twenty-first century scenario runs and concluded that ''twenty-first-century simulations may simply be too short for identification of significant tropical variability response to climate change.'' The present PGW approach allows us to largely bypass this issue and concentrate on aspects of the small-scale global warming climate signal.

Our calculations using the CMIP3 model results as the basis for future climate change were begun before some of the next generation CMIP5 model results were available. We do not feel that our use of results from global models that were state-of-the art circa 2006 represents a significant limitation. The most notable conclusion of studies that have compared the overall performance of the CMIP3 and CMIP5 models is the great degree of similarity of the CMIP3 and CMIP5 results. For example the suite of CMIP5 models display

only extremely modest overall improvements over CMIP3 in mean tropical rainfall distribution (Hirota and Takayabu 2013), mean cloud properties (Lauer and Hamilton 2013), and interannual SST variability (Wang et al. 2015).

c. *Paired t test*

We used a Student's *t* test to check if the present-day run and future run are statistically significantly different. Our null hypothesis is that the present-day run and the future run have the same climatological mean values; that is, the differences (present day minus future) are equal to zero. Since we consider the possibility of either positive or negative differences, we employed a ''double tailed'' *t* test. Furthermore, since the present-day run and the future run use the same base years (with and without adding the GWIs), we applied a ''paired *t* test'' (e.g., McDonald 2014). We applied the test to the time series of the annual means at each grid point.

3. Global warming results

In this section we will compare the results in the future 2080–99 HRCM simulation with those from the present-day 1990–2009 simulation. The main focus is on the results for the main Hawaiian Islands as represented in the intermediate domain with 3-km resolution, although we will also show some results for the island of Maui in the very fine-resolution innermost domain. Many results will be presented as the difference between the 2080–99 and 1990–2009 means; this represents the projected forced global warming signal over ~90 years, and we will refer to this difference as the projected future change or twenty-first-century change.

a. *Surface (2 m) air temperature (SAT)*

Figure 2a shows the HRCM simulated annual mean surface air temperature (SAT) averaged over 1990–2009. This quantity appears largely determined by the surrounding oceans and the local topographic elevation. Figure 2b presents the simulated future change of the annual mean SAT. Over the oceans the SAT increase closely follows the imposed SST warming. Over the land, however, a clear pattern of increasing warming with height is evident. It is notable that the observed SAT increase at Hawaii stations over the last few decades has also been found to be intensified at higher altitudes (Giambelluca et al. 2008). The projected future change of the near-surface air temperature increases nearly linearly with topographic elevation and the projected warming is ~3.5 K at the summits of Mauna Kea and Mauna Loa (Fig. 2b). Figure 2c shows the future change in annual mean SAT for individual land grid points plotted as a function of the topographic elevation.

An increase of projected greenhouse warming with height is found in the lowest few kilometers of the troposphere in global model simulations (e.g., Qu et al. 2015). The blue ''curve'' in Fig. 2c shows the air temperature increment from the CMIP3 multimodel mean used in our experiment, averaged around HRCM domain 2 (18°–23°N, 161°–154°W) and then interpolated vertically to the HRCM surface layer using the HRCM domain 2 terrain height. The surface warming over the land points of the HRCM is consistent with the air temperature increments from the CMIP3 multimodel mean. However, the realized SAT warming values at points below about 3-km altitude are about 0.1–0.3 K below the blue curve. This may be due to a trend for increased cloud cover over much of our domain in the future simulation. Also shown is the projected SAT increase at individual grid points sorted into those with high or low mean cloudiness [using the mean liquid water path (LWP) as a proxy, high means with LWP $> 200\,\mathrm{g\,m^{-2}}$ and low means with LWP $< 100\,\mathrm{g\,m^{-2}}$] in the present-day simulation (Fig. 2d; see caption for details). This shows that the projected surface warming is reduced particularly in cloudy areas that generally correspond to the windward side of each island. We will show below that the windward sides generally display increases in LWP and cloud cover in the warming projection.

Figure 3a shows histograms of daily mean SATs at the model grid point nearest the Honolulu airport weather station on the south shore of Oahu. Results are presented for the 20-yr present-day run and for 20-yr future run. Note that the spread of the SAT values shown includes the seasonal cycle as well as interannual variations and day-to-day weather fluctuations. The resolution of the histogram bins is 1°C and the peak value in the present-day run is for 25°–26°C (with 22% of all days), while in the late twenty-first-century simulation the peak is at 28°–29°C (with 23% of the days). Figures 3d,g,j show the same histograms but for three stations on the Big Island: Hilo near sea level on the windward side, Kulani Camp at a height of about 2.5 km on the windward side, and Mauna Kea station near Hawaii's highest summit [the locations of the stations are given in Table 2 and shown on a map in Zhang et al. (2016)]. The projected temperature increases are largest at Mauna Kea (about 4.2 km above sea level). In our 1990–2009 simulation about 35% of days feature daily minimum temperatures at the Mauna Kea summit that are below 0°C, a fraction that we project to drop to about 3% in the late twenty-first century.

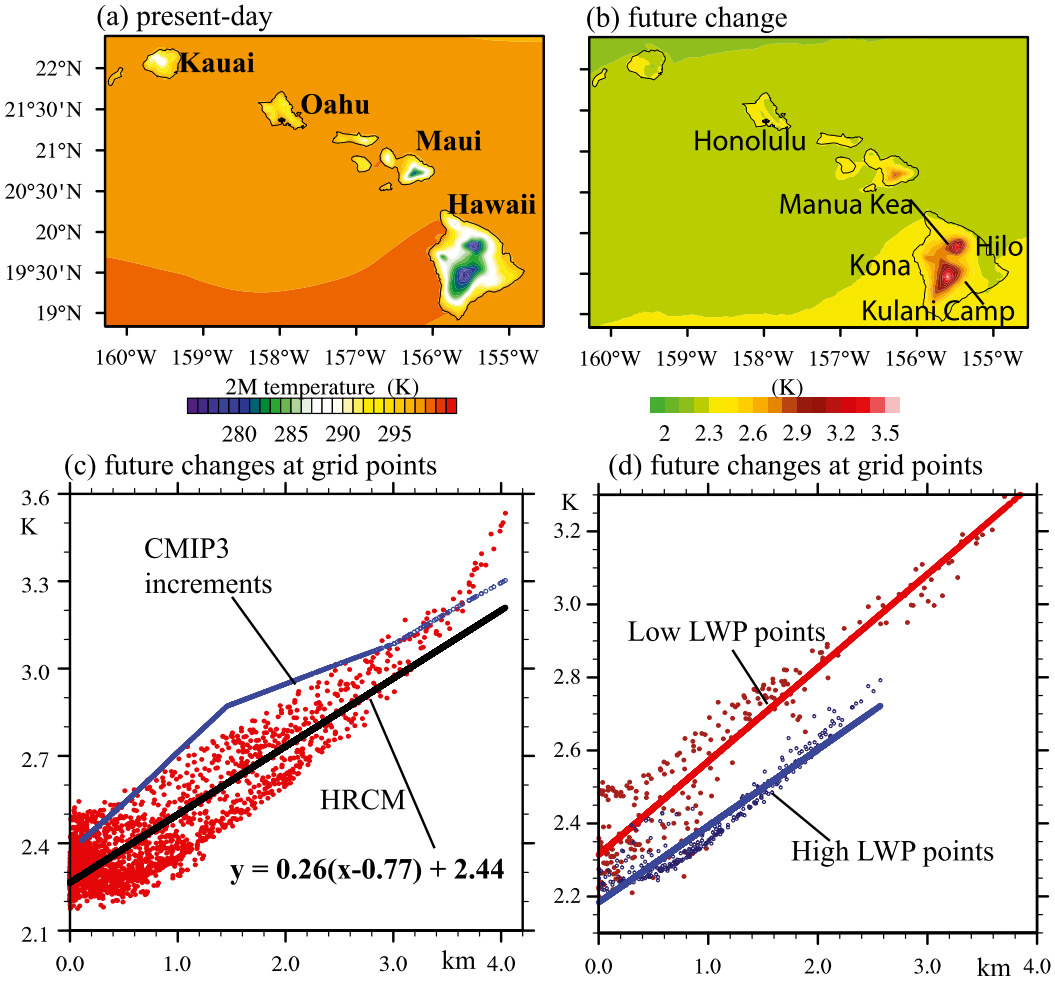

FIG. 2. The 20-yr mean surface air temperature for (a) present day and (b) future change. The future change is significant at the 99% confidence level. (c) The dots show the warming values at individual grid points plotted as a function of terrain height. The black line shows the least squares linear fit to the gridpoint data. The blue "curve" shows the height dependence of the warming increment from the CMIP3 multimodel mean (averaged around the area of domain 2 then interpolated to each model grid point). (d) Blue (red) points show the surface warming results for model grid points with high (low) annual mean LWP (high means with LWP $> 200\,\mathrm{g\,m^{-2}}$ and low means with LWP $< 100\,\mathrm{g\,m^{-2}}$; see also Figs. 5c,d) in the present-day simulation. The lines are linear fits to the points.

b. *Surface (10 m) wind speed*

The left panels of Fig. 4 show the seasonal mean climatology of surface wind speed in the present-day simulation (Figs. 4a,c) and the projected twenty-first-century changes (Figs. 4b,d). The present-day results are characterized by weaker winds over land than over ocean and in elongated "wind shadows" in the lee of the major mountains. The surface winds are particularly strong in the channels between the islands (notably the Alenuihaha Channel between Maui and the Big Island). In the global warming climate the wind speeds are nearly everywhere projected to increase, but the increases are relatively modest: less than $0.8\,\mathrm{m\,s^{-1}}$ over most of the ocean surface and considerably less over most of the land areas. The Big Island shows a somewhat different pattern of changes in wind anomaly from those in other areas, although the anomaly is very small and statistically significant only over parts of the island. Figures 4e–h are histograms of the daily mean wind speeds at grid points closest to the Honolulu Airport on Oahu and at Hilo Airport, Kulani Camp, and Mauna Kea summit on the Big Island. Results for the present day and the late twenty-first-century climate are compared. The histograms document a very modest increase in frequency of strong wind days at each station. We found that

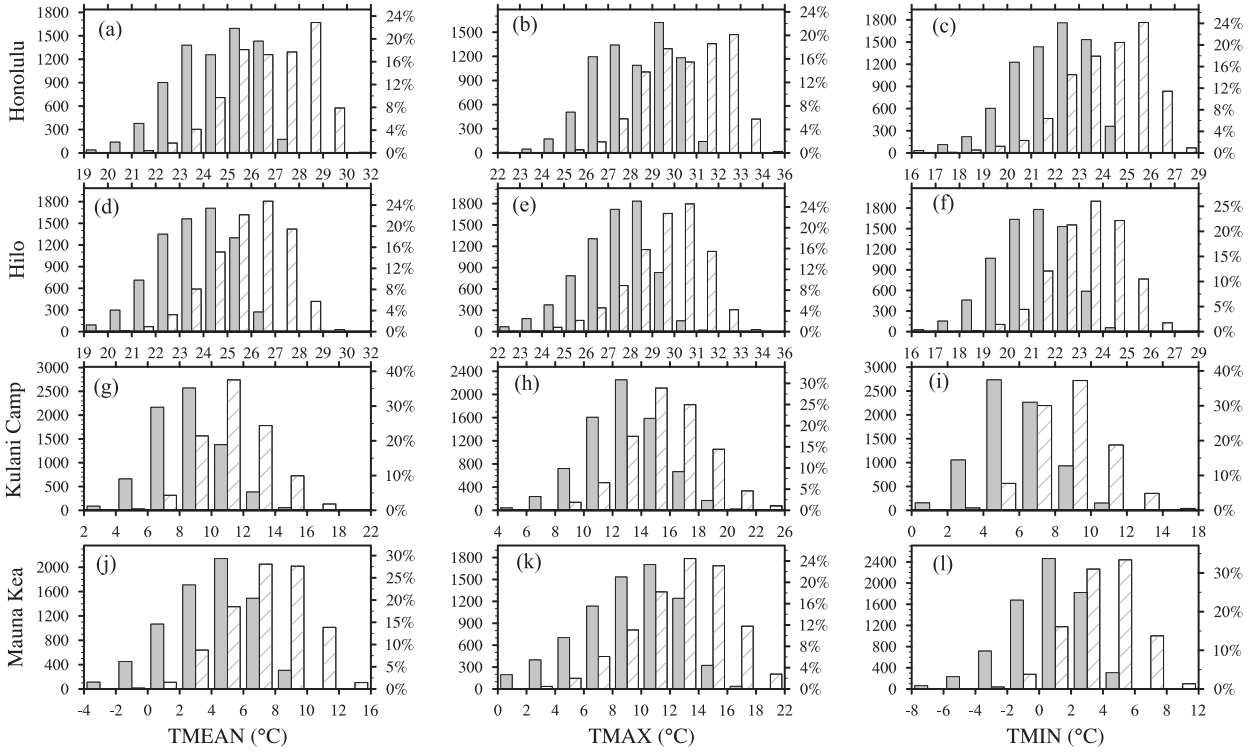

FIG. 3. The frequency of (from left to right) daily mean SAT, daily maximum SAT, and daily minimum SAT for present day (shaded) and future (hatched) at (from top to bottom) Honolulu airport, Hilo airport, Kulani Camp, and Mauna Kea summit. In each panel *y* axis to the left is the number of days and *y* axis to the right is percentage.

the modest increase in surface wind speed over the model domain is also seen in global coupled model results used to construct the GWI (not shown).

c. *Cloudiness and surface radiation*

The top panels in Fig. 5 display the present-day simulated mean total cloud fraction, mean LWP, and net shortwave radiation flux (NSWRF) at the surface. Figures 5b,d,f show the changes in these quantities in the late twenty-first-century simulation. The windward/leeward sides of the islands are generally associated with high/low mean cloudiness. The global warming change in cloudiness displays a rather similar geographical dependence with increased/decreased cloudiness on the windward/leeward sides in what could be very roughly characterized as ''cloudy regions get cloudier, clear regions get clearer'' pattern. However, because of the large interannual variability in cloudiness, the mean changes are statistically significant at the 99% confidence level only in some regions. Where cloudiness increases/decreases significantly in the warming climate there is generally a decrease/increase in NSWRF at the surface. The contrasts are particularly clear on the Big Island where the radiative flux is reduced by up to $\sim 15\,\mathrm{W\,m^{-2}}$ in some locations on the windward slopes of the northeast part of the island and are increased by $\sim 15\,\mathrm{W\,m^{-2}}$ at some places on the leeward slopes of the northwest part of the island. As noted above (Fig. 3) this contrast is accompanied by a ~0.2-K difference in realized SAT increases in the future climate simulation.

d. *Trade wind boundary layer structure*

The presence of a TWI is highly relevant as it will almost always preclude the possibility of a deep convective rainfall event. Zhang et al. (2012b, 2016) developed a procedure for defining those days with a marine boundary layer capped with a well-defined TWI. In such ''trade wind days'' we can generally identify a thin TWI cloud layer. For each trade wind day we compute boundary layer and boundary layer cloud parameters in the present-day and future simulations including cloud-base height (CBH), cloud-top height (CTH), and TWI-base height (TWIBH). Our procedure identifies 81% (80%) of soundings during 1990–2009 at Lihue (Hilo) as having clearly defined TWIs. Note that Cao et al. (2007) have analyzed the twice-daily radiosonde profiles from 1979–2003 at Hilo and Lihue and found that their own criterion for a well-defined TWI was satisfied slightly over 82% of the time at each station. Figure 6 compares the probability distribution functions (PDFs) of the

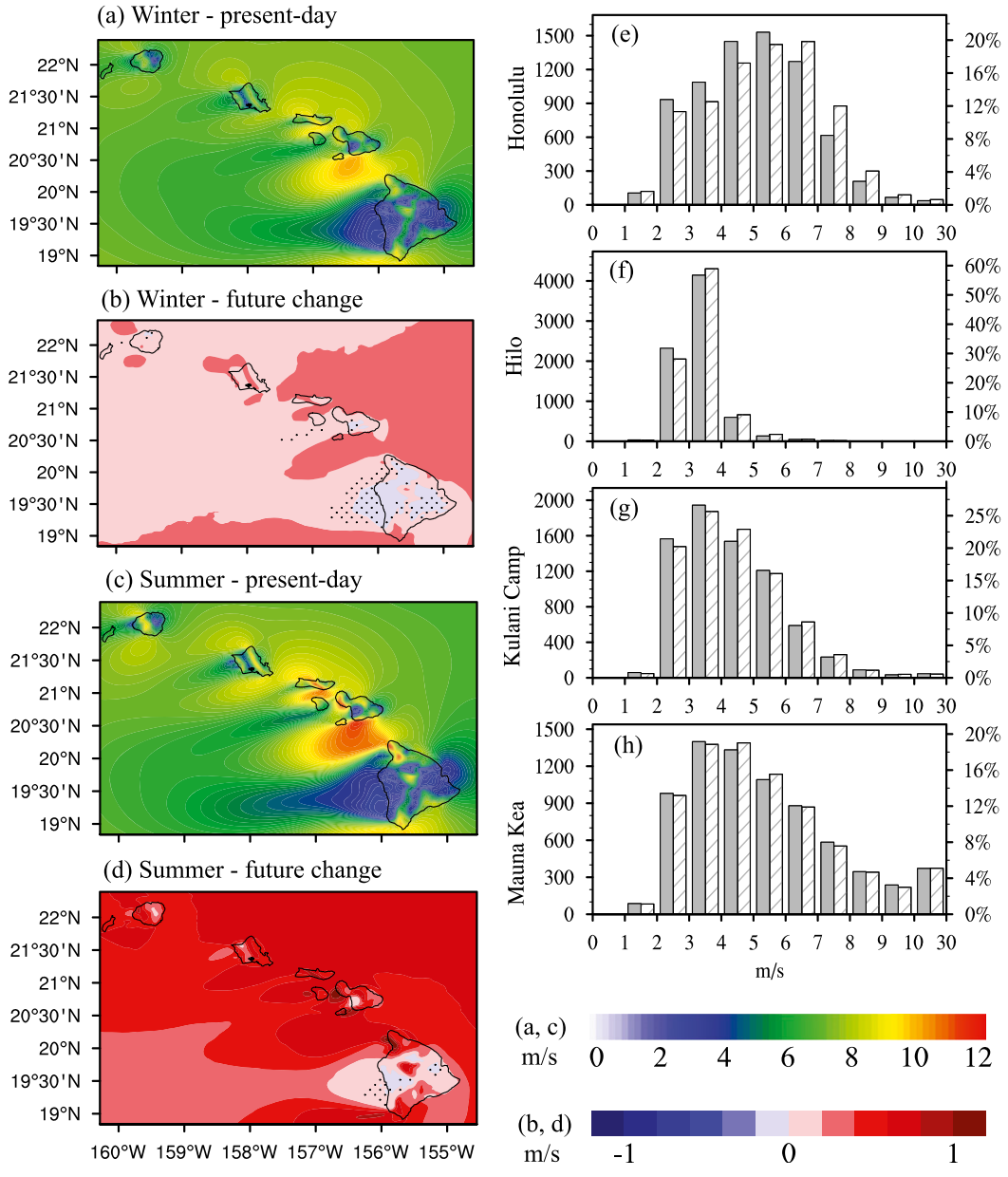

FIG. 4. The 20-yr seasonal mean surface (10 m) wind speed in (a),(c) the present-day simulation and (b),(d) the model's future change. The small gray dots in (b),(d) indicate that the future change is not statistically significant at the 99% confidence level. The frequency (the number of days to the left and the percentage to the right in the *y* axis) distributions of daily mean wind speed for present day (shaded) and future (hatched) at (e) Honolulu airport, (f) Hilo airport, (g) Kulani Camp, and (h) Mauna Kea summit.

TWIBH determined from radiosonde observations at Lihue and Hilo with those deduced from the present-day and future climate HRCM simulations. The distribution of TWIBH in the model simulation is quite similar to that in the observed profiles, although with an overall low bias in the model of somewhat over 100 m (a bias noted in Zhang et al. 2016). In the HRCM results for the future, the PDFs for the TWIBH do not change very much, but the frequency of TWI days increases from 83% to 92% (82% to 91%) at Lihue (Hilo). Figure 7a is a map showing the fraction of profiles displaying TWIs in the present-day HRCM simulation. The domain average (land and ocean) is also shown. The simulated TWI frequency is generally ~80%–85% at the windward edges of the islands. The values directly over the very high topography and leeward slopes of the Big Island in Fig. 7a may not be too

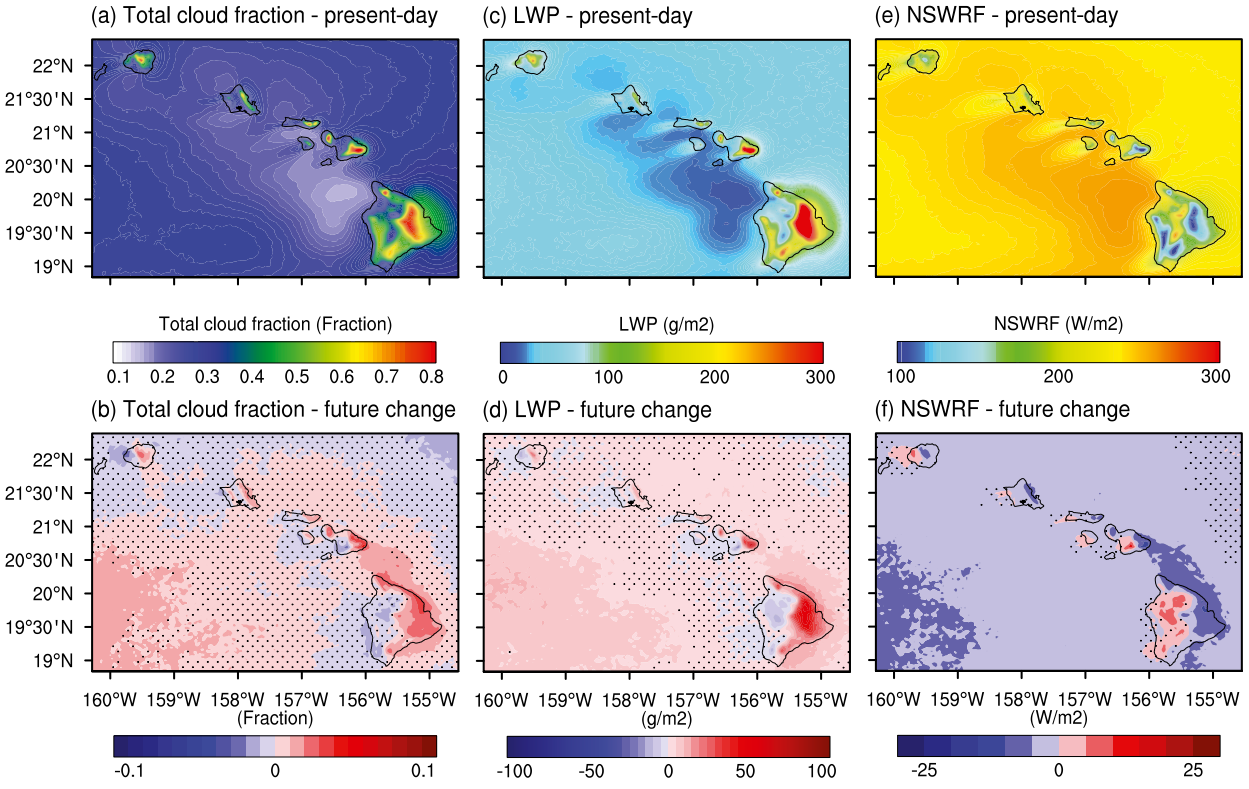

FIG. 5. The 20-yr mean total cloud fraction for (a) present-day simulation and (b) the modeled future change. (c),(d) As in (a),(b), but for LWP. (e),(f) As in (a),(b), but for NSWRF at the surface. The small gray dots in (b),(d),(f) indicate that the future change is not statistically significant at the 99% confidence level.

meaningful, but the flow of the air over topography appears to have some effect and the TWI criterion is met only ~75%–80% of the time at some locations in the lee of the major islands. The mean value for the domain is 83.2%. Figure 7b shows the change in TWI occurrence in the future simulation. This increase averages 8% over the whole domain and the increase is generally slightly larger over the islands themselves. This change in TWI frequency corresponds to a very large relative decrease in the fraction of days without a well-defined TWI—for example, from ~17% in the present to ~9% in the future. As noted earlier, the presence of a TWI will generally prevents deep convective rainfall events, and so the model simulation indicates that in the global warming scenario there will be fewer days with the possibility of deep convection.

Figure 8 shows the changes in annual mean values for CBH, CTH, and TWIBH averaged over all days with a well-defined TWI. The projected changes in all of these average quantities are quite modest: generally less than ~0.04 km at most individual locations and only about 0.01 km in the domain average, changes actually less than the model level spacing near the TWI (0.15–0.3 km) with most of the changes not being statistically significant throughout the model domain (see Fig. 8). The overall impression is that the marine boundary layer structure around Hawaii will not change much with global warming but that the frequency of days with a well-defined marine boundary layer topped with a TWI will significantly increase.

e. *Mean rainfall*

The left panels in Fig. 9 show 1) the simulated mean rainfall rate averaged over the full 20-yr present-day HRCM simulation, 2) the change in this mean rainfall rate in the future climate simulation, and 3) this change expressed as a fraction of the present-day mean value at each location. The middle and right panels of Fig. 9 show the same quantities for the "winter" (November–April) and "summer" (May–October), respectively. The comparison of the present-day HRCM results with observations is discussed extensively in Zhang et al. (2016), but note here that the major features of the observed mean rainfall are captured in the simulation—notably rainy windward slopes on all islands, generally dry leeward rain shadow areas, the very wet summit on Kauai, and the two very dry summits on the Big Island (Mauna Kea and Mauna Loa).

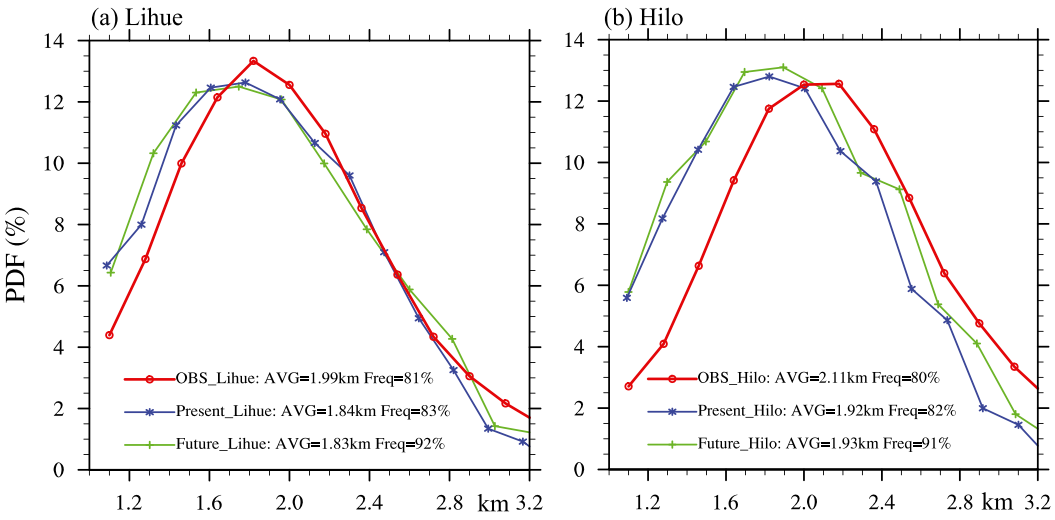

FIG. 6. The PDFs for the TWIBH at (a) Lihue and (b) Hilo from the radiosonde observations (1990–2009) and in the present-day and global warming HRCM simulations. Results in each case computed using only profiles that showed a clear TWI and the mean frequency of occurrence of such profiles is given for each case along with long-term mean TWIBH.

In the simulated warmer climate there are substantial changes (10%–40%) in the mean rainfall at many locations over the islands. There are strong horizontal gradients in the climatological rainfall in Hawaii and the simulated changes in rainfall also display strong horizontal variations. Generally there are reductions in rainfall in the rain shadow areas and increases on the windward slopes. Overall the changes seem roughly consistent with a ''wet regions get wetter'' and ''dry regions get drier'' pattern that is also seen as typical in global model projections of greenhouse warming (e.g., Held and Soden 2006). In the latest IPCC review Collins et al. (2013) state that there is ''high confidence that the contrast of seasonal mean precipitation between dry and wet regions will increase in a warmer climate over most of the globe.'' The patterns of projected change in Fig. 9 are fairly similar in winter and summer. Perhaps the most striking seasonal dependence is the larger increase in rainfall on the windward slopes of the Big Island in summer (up to ~40%) than in winter (up to ~20%).

The warmed climate simulation shows increased rainfall in places with strong orographic rainfall in the present day. A possible explanation of this would be simply that increased air temperatures will lead to increased moisture in the lower atmosphere, which then flows off the oceans and over the orography of each island. This is basically consistent with the results of the detailed analysis of the water vapor convergence in the lower atmosphere presented in the next subsection. The reduction in rainfall in the normally dry rain shadow areas may be explained by the reduction in non-TWI days in the warm climate and consequent reduction in the number of days with opportunity for deep convective rainfall events to form. Qu et al. (2015) examined responses to mean warming in the tropical lower atmosphere in several different global models. They note that the increase of warming with height in each model they analyzed is large enough that the moist stability of the lower atmosphere is increased. Our HRCM results with apparently less deep convective rainfall over Hawaii may be generally consistent with Qu et al.'s (2015) finding of an overall increase in average tropical moist stability under global warming.

f. Convergence of boundary layer moisture flux

In the long-term mean, the rainfall rate at any point on the surface should equal the vertically integrated atmospheric moisture flux convergence plus the local evapotranspiration. At low latitudes the vertical integral of the moisture convergence is generally dominated by the contribution in the boundary layer (Kuo 1965, 1974). The vertically integrated boundary layer moisture flux convergence bMFC can be written as follows:

$$\mathrm{bMFC} = -\frac{1}{g}\int_{P_{\mathrm{sfc}}}^{P_{\mathrm{bl}}} \nabla\cdot(qV_h)\,dp, \qquad (1)$$

where g is the gravitational acceleration, p is pressure, P_{sfc} is the surface pressure, and P_{bl} is the pressure at the top of the boundary layer, which for our

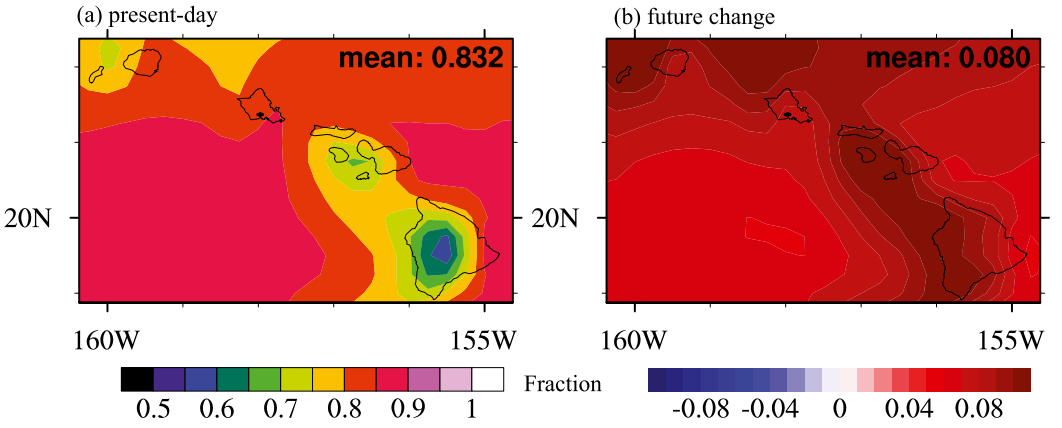

FIG. 7. (a) The 20-yr annual mean TWI frequency in the present-day simulations. (b) The future change in TWI frequency in the model projection. The future change is statistically significant at the 99% confidence level throughout the domain.

calculations here we have approximated simply to be $P_{\mathrm{bl}} = P_{\mathrm{sfc}} - 400\,\mathrm{hPa}$.

In this project we calculated the portion of bMFC attributable to the monthly mean fields. We define

$$q = \overline{q} + q', \quad V_h = \overline{V_h} + V_h', \tag{2}$$

where q is the specific humidity in the future simulation and $\overline{q}$ is the specific humidity in the present-day simulation so that q' represents the future change. All quantities are monthly means. A similar decomposition is applied for the horizontal wind speed V_h. Combining (1) and (2), we get the following:

$$\underbrace{\mathrm{bMFC}_{\mathrm{future}} - \mathrm{bMFC}_{\mathrm{present}}}_{\text{future change}} = \left[\underbrace{-\frac{1}{g}\int_{\mathrm{Psfc}}^{\mathrm{Pbl}} \nabla\cdot(qV_h)\,dp}_{\text{future}}\right] - \left[\underbrace{-\frac{1}{g}\int_{\mathrm{Psfc}}^{\mathrm{Pbl}} \nabla\cdot(\overline{q}\,\overline{V_h})\,dp}_{\text{present-day}}\right]$$

$$= \underbrace{-\frac{1}{g}\int_{\mathrm{Psfc}}^{\mathrm{Pbl}} \nabla\cdot(q'\overline{V_h})\,dp}_{\text{term1}} \underbrace{-\frac{1}{g}\int_{\mathrm{Psfc}}^{\mathrm{Pbl}} \nabla\cdot(\overline{q}V_h')\,dp}_{\text{term2}} \underbrace{-\frac{1}{g}\int_{\mathrm{Psfc}}^{\mathrm{Pbl}} \nabla\cdot(q'V_h')\,dp}_{\text{term3}}, \tag{3}$$

The term1 represents the perturbation of bMFC due to the change in long-term mean specific humidity, term2 represents the change of bMFC due to the difference of wind speed, and *term3* is due to the nonlinear interaction of differences in both quantities. In our analysis monthly mean winds and specific humidity are used in the calculations so contributions by transient eddies contributions are not included.

Figure 10 shows the 20-yr mean of each term of (3) averaged over the summer months. The topography causes intense convergence (windward side) and divergence (leeward side) over the Hawaiian Islands compared to the open ocean (Fig. 10a). The pattern of the bMFC over the land areas is similar to the corresponding pattern of summer mean (Fig. 9g) rainfall. The change in bMFC in the warmed climate (Fig. 10b) resembles the projected change in rainfall (Fig. 9h) with the overall tendency for wet-gets-wetter/dry-gets-drier conditions. This quantity is decomposed into term1, term2, and term3 in Figs. 10c, 10d, and 10e, respectively. It is apparent that term1, which expresses the change in bMFC due to change in mean boundary layer absolute humidity, strongly dominates the other terms. We find that changes in boundary layer RH in the global warming simulation are small (~1%–2%), and so the absolute humidity in the climate change simulation is enhanced by changes in the saturation humidity. The expected rate for this is ~7% $(^{\circ}\mathrm{C})^{-1}$ of warming (e.g., Held and Soden 2006). Given a reasonably smooth map of increase of mean warming, the

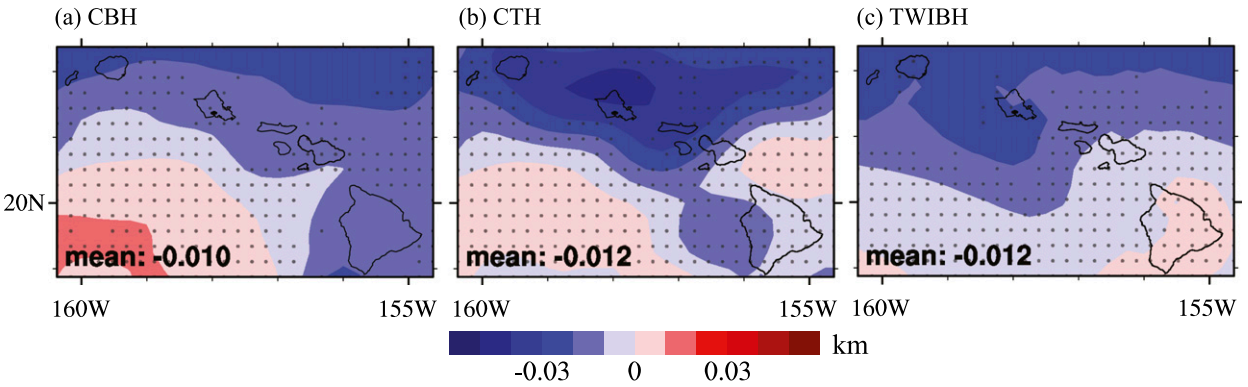

FIG. 8. The future change for annual mean (a) CBH, (b) CTH, and (c) TWIBH. The gray dots indicate that the future change is not statistically significant at the 99% confidence level.

term1 will largely be an enhancement of the present day local convergence or divergence. The notion that the wet-gets-wetter/dry-gets-drier precipitation changes may be driven to first order by this enhancement of horizontal moisture transports has been widely applied in interpreting global warming simulations (e.g., Held and Soden 2006). In our simulations this easily understood effect dominates the changes in bMFC attributable to alteration of the mean circulation in the boundary layer, and it can account for the basic pattern of mean precipitation changes due to global warming.

g. *Rainfall extremes*

Flooding sparked by individual rainfall episodes is a practical concern in Hawaii with floods causing significant disruption somewhere in Hawaii virtually every year and with many years featuring quite destructive flooding (e.g., Cram and Tatum 1979; Tu and Chen 2011; http://www.floodsafety.noaa.gov/states/hi-flood.shtml). As an example, one flooding event caused by quite localized heavy rainfall for a few hours in east Oahu on 30 October 2004 caused about $100 million in damages (http://www.prh.noaa.gov/hnl/pages/events/ManoaFlood 20041030).

As the mean climate warms we can expect changes in extreme rainfall events as well as in mean rainfall. How rainfall extremes may change under global warming has been investigated in a number of global model studies. Kharin et al. (2007) examined results for daily rainfall amounts in a large number of coupled global climate model simulations and found extremes generally became enhanced in a warmer climate, with both ''increased intensity of precipitation extremes'' and ''[reduced] waiting times for late-twenty-first-century extreme precipitation events ... almost everywhere'' in a warmer climate. O'Gorman and Schneider (2009) also found a general enhancement of daily rainfall extremes in warming simulations with 11 different coupled global models, but the degree of enhancement for given mean surface warming varied significantly among the models.

Figure 11a shows the 90th percentile of daily rainfall during 1990–2009 plotted over all the islands based on measurements from 137 rain gauge stations (locations shown on the figure). Each day's rainfall accumulation was mapped onto the 1891 land grid points of the HRCM 3-km mesh using Cressman interpolation (Cressman 1959; Zhang et al. 2016). The interpolated observed values were then used to determine the 90th percentile boundary at each grid point. This percentile boundary is generally largest at the locations with heaviest mean rainfall and exceeds 50 mm day^{-1} near the highest topography on Kauai and at locations on the windward slopes of the Big Island. The somewhat noisy map in Fig. 11a may reflect the limited station coverage, but the overall pattern on each major island seems clear. Figure 11b shows the same quantity calculated at each of the 1891 land grid points in the 20-yr present-day simulation with the 3-km-resolution HRCM. The model results are smoother than the interpolated observations but display an overall similar pattern with large values for the percentile boundary on the windward slopes of the Big Island. There also are some systematic biases in the model, notably with the peak values on the Big Island being larger than observed and the values on Oahu being smaller than observed. These differences resemble those in the mean rainfall rate itself. Zhang et al. (2016) showed that the HRCM rainfall has an overall dry bias on Oahu and a wet bias on the windward slopes of the Big Island.

Figure 11c shows the change in the 90th percentile boundary in the global warming simulation. We see modest reductions in this value over much of the islands but significant increases in places with heavy mean rainfall, notably the windward slopes of the Big Island and Maui and the high topography of Kauai. The overall

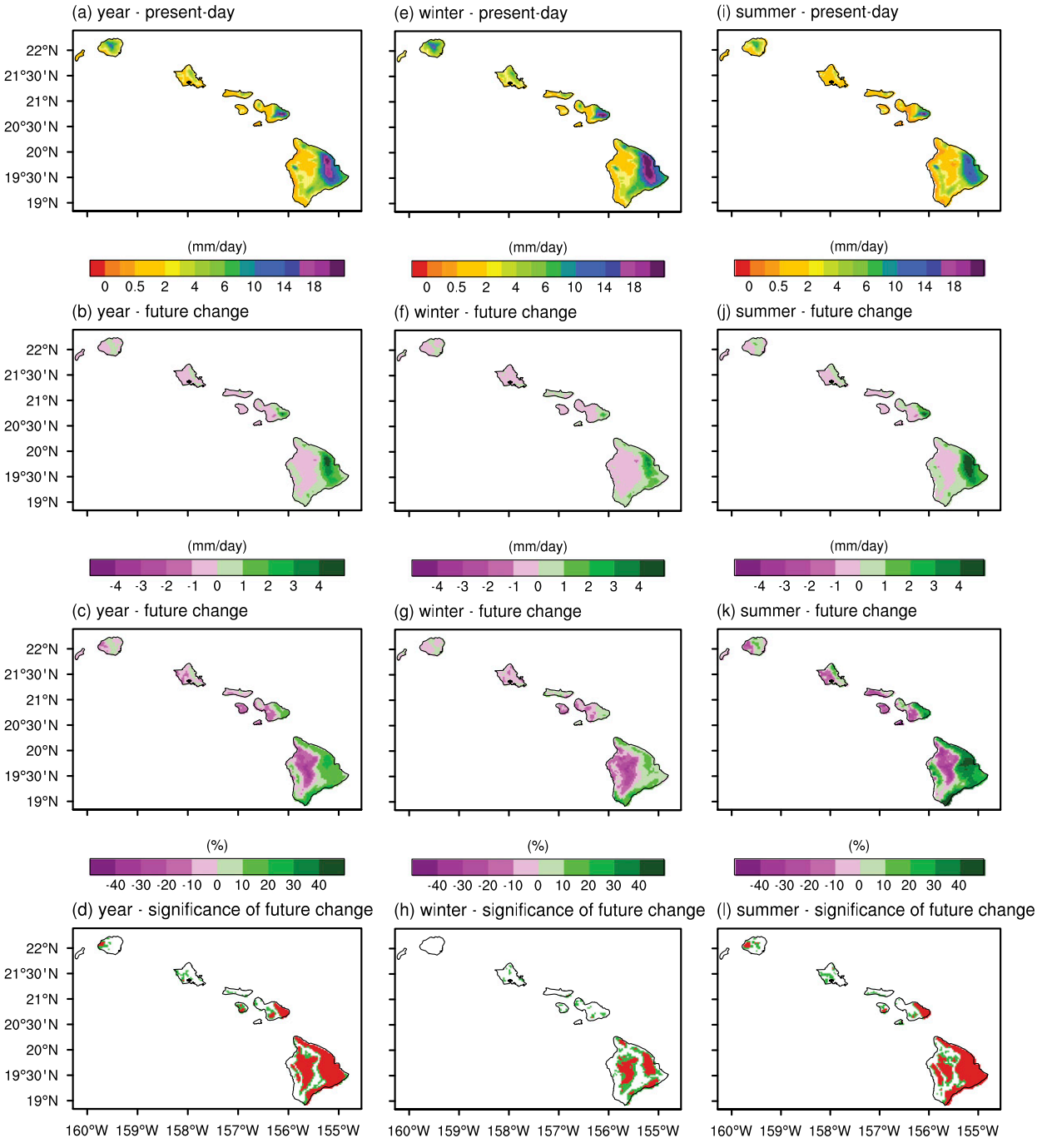

FIG. 9. The 20-yr mean precipitation for the (a) whole year, (e) winter, and (i) summer in the present-day HRCM simulation. The future change (mm day^{-1}) of precipitation for (b) annual mean, (f) winter mean, and (j) summer mean. The future change expressed as a fraction of the present-day simulated climatological values shown for (c) annual mean, (g) winter mean, and (k) summer mean. Shaded areas indicate that the future change is statistically significant at the 99% confidence level (red) and the 90% confidence level (red + green) for (d) year, (h) winter, and (l) summer, respectively.

patterns noted above are also seen in Figs. 11d,e,f, which repeat the analysis of observations, present-day simulation, and projected future change for the 99th-percentile boundary of daily rainfall.

The HRCM global warming simulations show that the percentile boundaries increase in those areas with heaviest mean rainfall. This suggests that the most extreme rainfall events seen anywhere across the entire state will

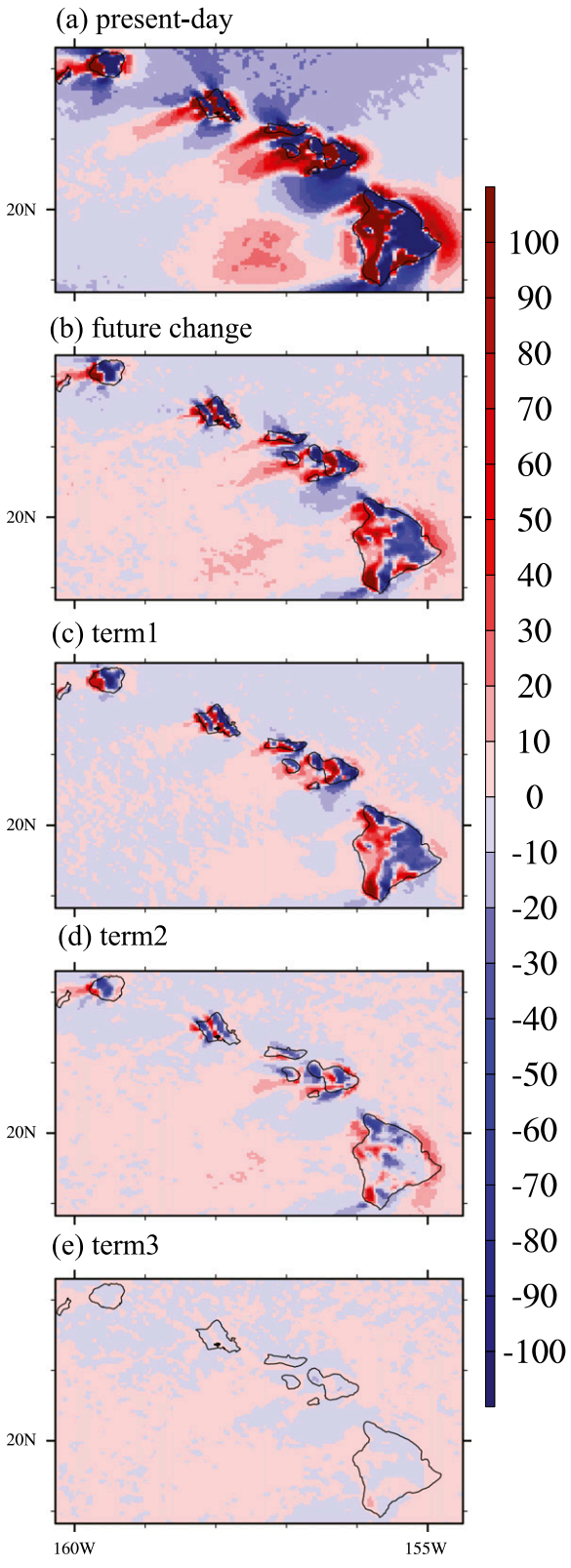

FIG. 10. The 20-yr summer mean of the low-level moisture convergence breakdown terms in (3). The unit is 10^{-4} kg m^{-2} s^{-1}.

be enhanced in the future climate. Figure 12 addresses this by displaying HRCM results for daily rainfall extremes aggregated over all the land grid points and all days through the 20-yr runs. The blue bars show results from the present-day simulation. These can be compared with the thin black bars that show the same quantities calculated from all available station data during 1990–2009 but then scaled by the number of gridpoint days (1891 times 7305 days = 13 813 755) in the model simulation divided by the number of available station days of observations (915 865). Since the stations have an irregular geographical distribution the comparison is not precise, but the results do provide some validation of the HRCM simulated rainfall extremes. The red bars show the results for the HRCM global warming simulation. The extreme daily rainfall events are more common in the global warming simulation for every rainfall range > 50 mm day^{-1}. The result is particularly striking for the most extreme events (e.g., >500 mm day^{-1}), which are more than twice as frequent in the warmed climate projection. Figure 13 shows the same analysis applied to hourly rainfall in both observations and the HRCM simulation. Once again a large enhancement of the most extreme hourly rainfall events is evident in the warming climate.

h. Results for 1-km domain over Maui

Results thus far have only been shown for the 3-km-resolution intermediate domain. As noted above in section 2, both the present-day (1990–2009) and future (2080–99) HRCM simulations were performed with a third, one-way nested, innermost domain that covers the island of Maui and adjacent regions with 1-km horizontal resolution. While Zhang et al. (2016) show that the 3-km resolution in the HRCM simulates the basic features of the present-day geographical distribution of climatological rainfall, they also noted some biases, particularly on the island of Maui. They speculated that it might be directly connected with the finite representation of the very steep topography characteristic of this island. Zhang et al. (2016) showed that the simulation over Maui in the 1-km-resolution innermost domain does indeed produce a substantially improved simulation of the mean rainfall distribution.

Figure 14a shows the relative change in mean annual rainfall rate over Maui and environs in the future simulation compared with the present-day simulated climatology computed for the land grid points of the innermost 1-km domain. Figure 14b shows the same quantity for the same geographical area but computed from the 3-km intermediate domain simulation (so Fig. 14b effectively represents a detail from Fig. 9c above, although note the different color bars used for the shading). The overall pattern of increased rainfall

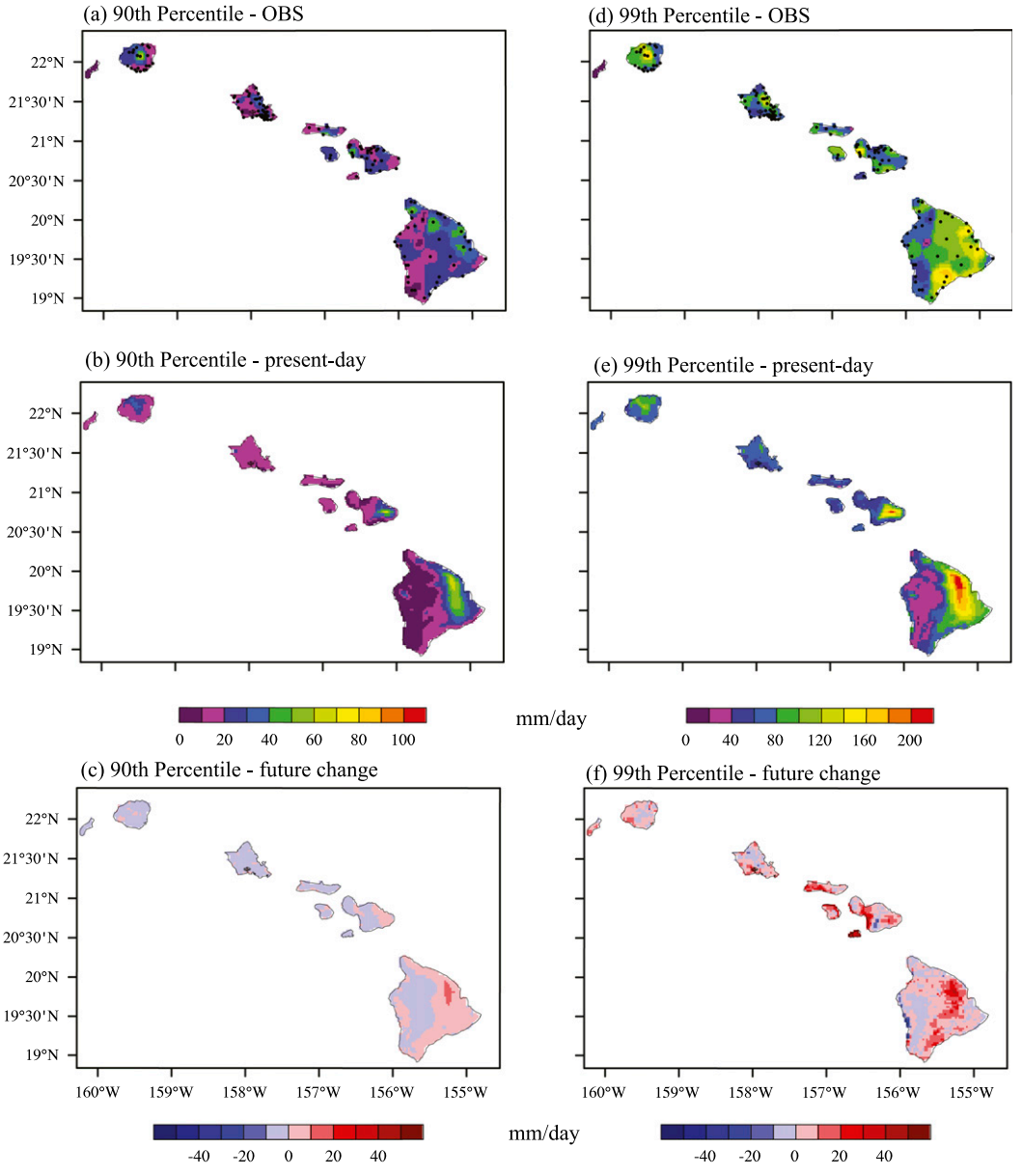

FIG. 11. (a) The 90th-percentile threshold of daily precipitation at each location based on station rain gauge observations for 1990–2009. (b) As in (a), but from the present-day simulation with HRCM. (c) The change in the 90th-percentile threshold in the future climate simulation. (d)–(f) As in Figs. 9a–c, but for the 99th percentile of daily precipitation. The black dots in (a),(d) show the locations of the observational stations.

on the wet windward sides of east Maui and reduced rainfall in the rain shadow leeward area is apparent in both simulations. However, the details between the two resolutions are different, with the 1-km version showing enhancement of the projected increases in the mean rainfall on the east facing windward slopes of east Maui and near the highest topography at the center of west Maui. This enhancement to the wet-gets-wetter response in the 1-km-grid version mirrors to some extent the differences in the mean present-day rainfall itself as simulated in the 3- and 1-km HRCM domains (see Fig. 13 of Zhang et al. 2016). The dry-gets-drier pattern is notably enhanced in the 1-km simulation over Kahoolawe, the small island that occupies the southwest corner of the innermost domain. Kahoolawe, which is located in the usual rain shadow leeward of Maui, is known for its very dry conditions and our projection is for even less rainfall there under global warming conditions.

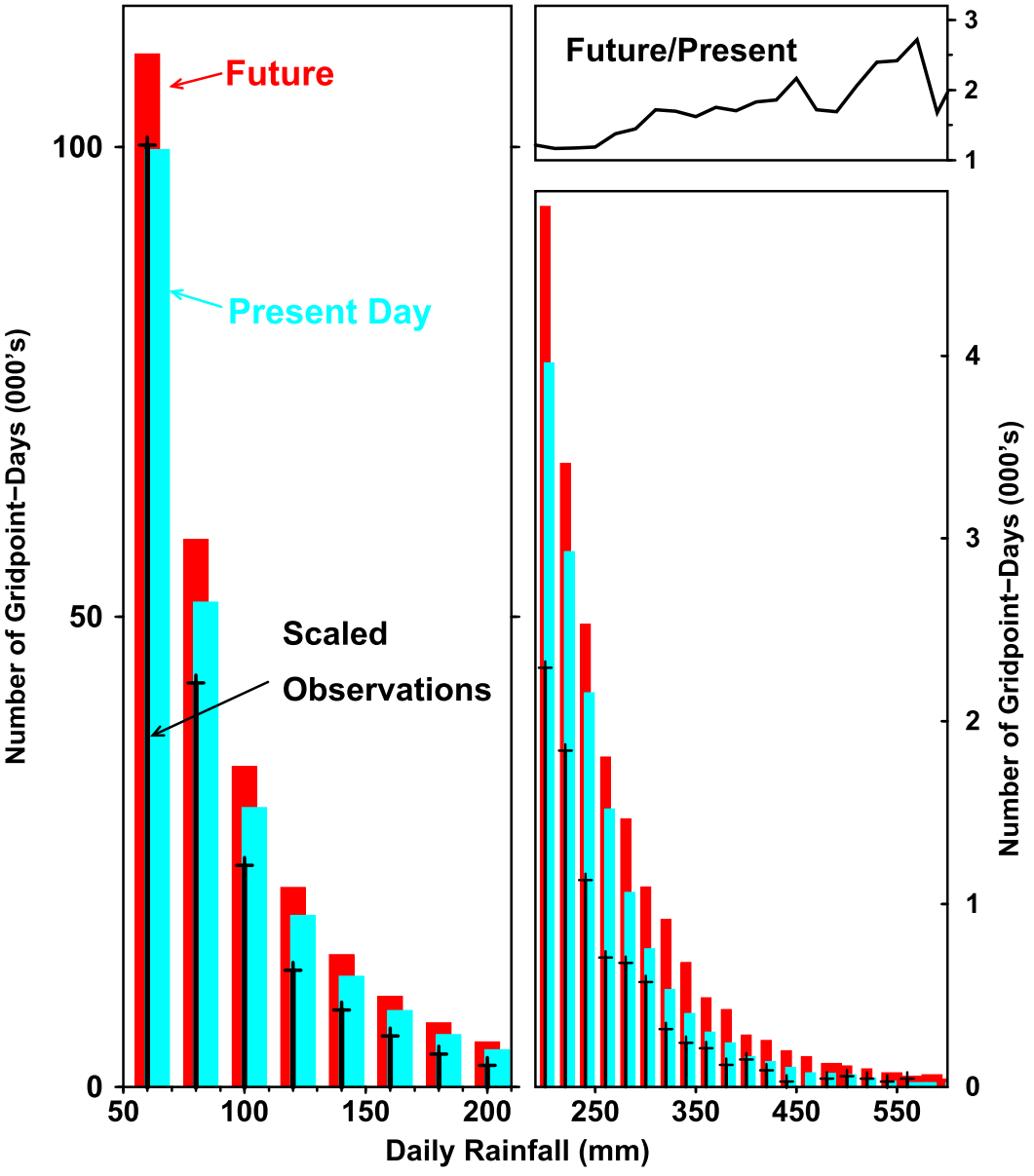

FIG. 12. Histogram of daily precipitation amounts greater than 50 mm during 20 years, sorted in 20-mm bins. Blue bars for the present-day HRCM simulation and red bars for the HRCM future simulation. These values are computed for all 1891 land grid points in the 3-km HRCM grid. The black crosses show results for 137 rain gauge stations in Hawaii with long records during 1990–2009. The observed results are multiplied by the total number of land gridpoint days in each model simulation divided by the number of individual station days available. (top right) The ratio of the future to present-day frequencies from the model simulations plotted for amounts > 200 mm.

4. Conclusions

This paper has described the changes in climate projected at fine resolution over the Hawaiian Islands based on a regional atmospheric model forced by the PGW method with boundary conditions based on earlier global coupled model projections of twenty-first-century anthropogenic warming. While there are many limitations in our model and experimental setup, our study represents a first attempt at climate projection with a physical model that resolves the microclimates of Hawaii. While recognizing the uncertainties associated with the somewhat preliminary nature of our projection, we have tried to make it as useful as possible as potential input for climate change impact and adaptation planning issues in Hawaii. The driving for our projection is based on a multimodel mean of standard global model climate simulations made assuming future emissions are from

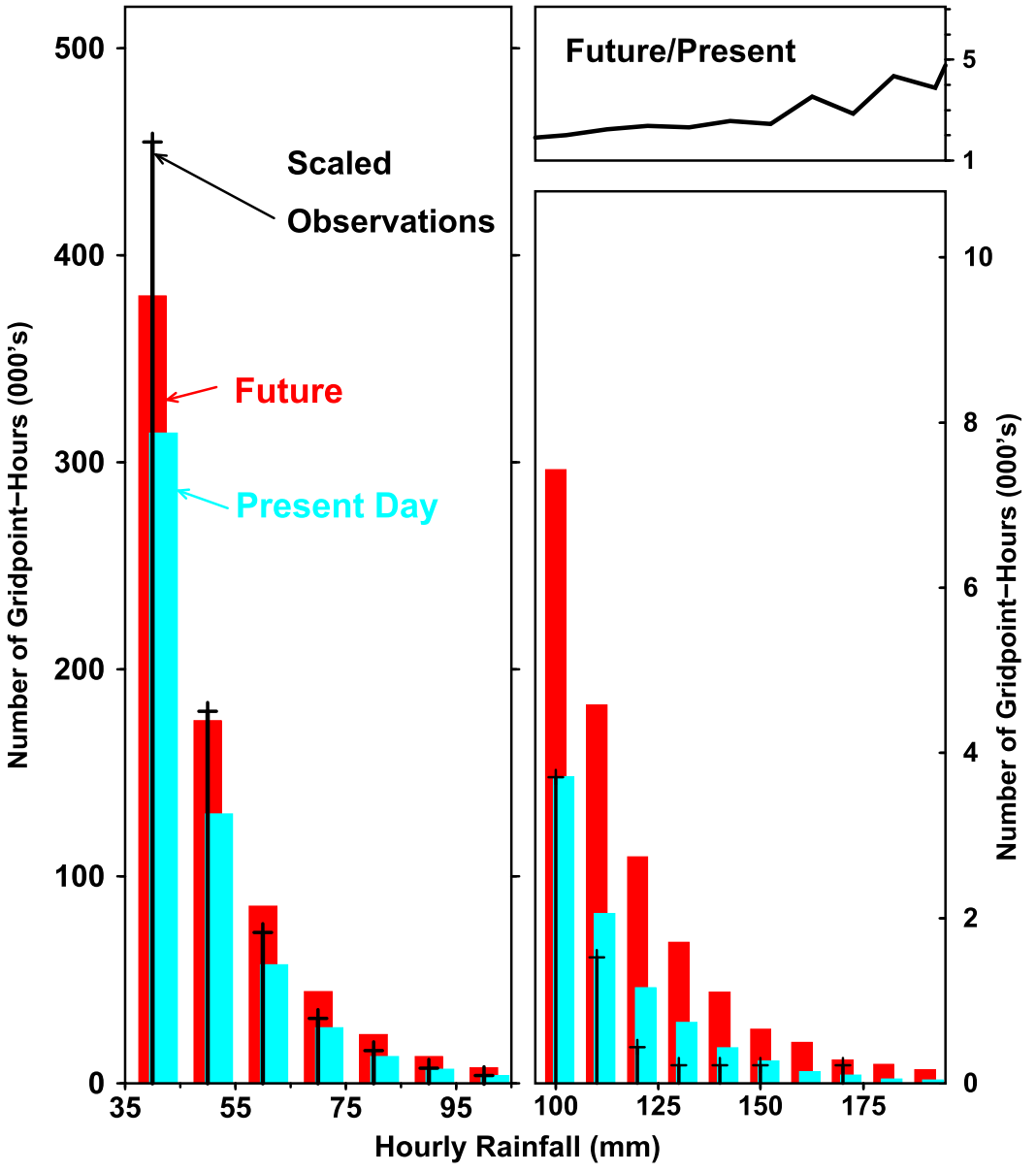

FIG. 13. As in Fig. 12, but for hourly precipitation amounts greater than 35 mm and sorted into 10-mm bins. (top right) The ratio of the future to present-day frequencies from the model simulations plotted for amounts > 95 mm.

SREAS A1B, a scenario that has been adopted in many earlier studies as representing a ''middle of the road'' economic projection.

Our model results suggest that the following changes relative to conditions around the year 2000 should be anticipated by the end of the twenty-first century:

(i) A warming of the surface atmosphere of 2°–3.5°C, with largest surface warming at the highest elevations.
(ii) Modest changes in the overall atmospheric circulation but with a general strengthening of surface winds in most localities.
(iii) Significant changes in mean cloudiness and mean rainfall, but with these changes strongly varying within each of the major islands. In particular the areas that in the present day are notably cloudy and rainy are generally projected to become cloudier and rainier, while dry sunny regions become even less cloudy and less rainy. The practical effects of reduced rainfall in currently dry areas will likely be exacerbated by increased potential evapotranspiration partially due to increased SAT and may lead to significant problems for freshwater resources in these regions (e.g., King 2014).

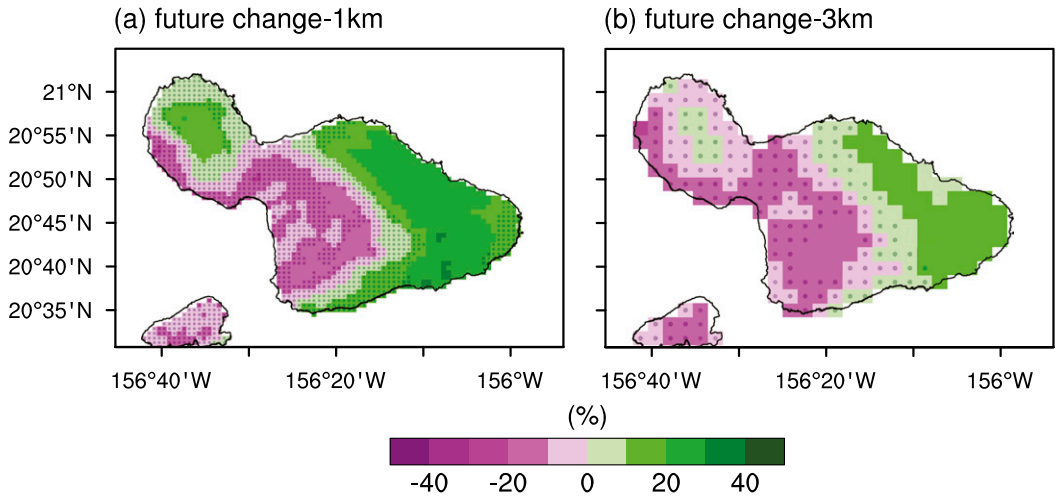

FIG. 14. The future change in annual mean rainfall rates expressed as a fraction of the present day (1990–2009) simulated climatological values. Results in (a) 1- and (b) 3-km HRCM grids over Maui and the island of Kahoolawe (southwest corner). The gray dots indicate that the future change is not statistically significant at the 99% confidence level.

(iv) A significant enhancement to the heaviest local rainfall events with implications for the frequency and severity of flooding. These enhanced extreme rainfalls will act in concert with rising sea levels driven by global climate change to intensify flooding of low-lying localities in Hawaii (Kane et al. 2015).

Of course the present model simulations aim to predict just the climate response forced by the anthropogenic changes included in the SRES A1B global model projections. The 2080–99 minus 1990–2009 changes in the real world (or in any single model realization) will also have a component from natural variability that is not predictable. Seasonal rainfall over the Hawaiian Islands is correlated with the state of the Southern Oscillation and is also controlled to some extent by lower-frequency regional ocean–atmosphere variability such as the Pacific decadal oscillation (Chu and Chen 2005). The use of 20-yr means to characterize the climate in our simulations will reduce, but not eliminate, sampling noise in our projection of long-term forced trends. Our use of the PGW approach will limit the effects of interannual variability on the results and help isolate the forced component of climate change. The downside of the PGW approach is an unrealistic constraint on the interannual and other internal variability in the future climate simulation. While this means that our exploration of future climate change is incomplete, we feel that our experiments do reliably identify a robust and significant component of expected climate change for Hawaii. Our most basic findings of surface warming intensified with topographic height and increased mean orographic rainfall on the windward slopes associated with increased water vapor in the boundary layer can be explained by simple mechanisms that should not depend strongly on details of the global or regional models employed.

Our future work will focus on improving our approach through finer model spatial resolution and other possible modifications to the HRCM model formulation. We will also apply our techniques to climate simulation and climate change projection for other tropical Pacific islands. We plan experiments to assess the limitations of the PGW approach adopted here and the effects of including ensemble integrations. Such experiments might include randomly perturbing the global warming increments used in the boundary forcing. We also propose to evaluate the PGW method within a ''perfect model'' context—that is, downscaling a global warming simulation from a single coupled GCM and then comparing results with a PGW approach using the present-day GCM simulation as the base. We also expect to collaborate with colleagues who will apply our projections to examine various practical effects of global warming on the natural and human systems on Hawaii and other tropical islands.

Acknowledgments. This study was supported in part by the NOAA Pacific RISA program via a subcontract from the East-West Center to the University of Hawaii and in part by the Department of Interior Pacific Islands Climate Science Center Agreements G12AC20501 and G13AC00363 awarded through the U.S. Geological Survey. The Pacific Islands Climate Change Cooperative

provided support through U.S. Fish and Wildlife Service Grant 12200AJ022. Additional support was provided by the Japan Agency for Marine-Earth Science and Technology (JAMSTEC), which sponsors research at IPRC. We would like to acknowledge the Hawaii Open Supercomputer Center (HOSC) for providing access to their facilities. We thank three anonymous reviewers for their comments and suggestions.

APPENDIX

Abbreviations

20C3M	Twentieth-Century Climate in Coupled Models
bMFC	Vertically integrated boundary layer moisture flux convergence
CBH	Cloud-base height
CMIP	Coupled Model Intercomparison Project
CTH	Cloud-top height
GWI	Global warming increment
HRCM	Hawaiian regional climate model
IPCC	Intergovernmental Panel on Climate Change
LWP	Liquid water path
NSWRF	Net shortwave radiation flux
PGW	Pseudo-global-warming method
SAT	Surface 2-m air temperature
TWI	Trade wind inversion
TWIBH	Trade wind inversion–base height

REFERENCES

Ashfaq, M., C. B. Skinner, and N. S. Diffenbaugh, 2011: Influence of SST biases on future climate change projections. *Climate Dyn.*, **36**, 1303–1319, doi:10.1007/s00382-010-0875-2.

Benning, T. L., D. LaPointe, C. T. Atkinson, and P. M. Vitousek, 2002: Interactions of climate change with biological invasions and land use in the Hawaiian Islands: Modeling the fate of endemic birds using a geographic information system. *Proc. Natl. Acad. Sci. USA*, **99**, 14 246–14 249, doi:10.1073/pnas.162372399.

Bothwell, L. D., P. C. Selmants, C. P. Giardina, and C. M. Litton, 2014: Leaf litter decomposition rates increase with rising mean annual temperature in Hawaiian tropical montane wet forests. *PeerJ*, **2**, e685, doi:10.7717/peerj.685.

Cao, G., T. W. Giambelluca, D. E. Stevens, and T. A. Schroeder, 2007: Inversion variability in the Hawaiian regime. *J. Climate*, **20**, 1145–1160, doi:10.1175/JCLI4033.1.

Chu, P.-S., and H. Chen, 2005: Interannual and interdecadal rainfall variations in the Hawaiian Islands. *J. Climate*, **18**, 4796–4813, doi:10.1175/JCLI3578.1.

——, A. J. Nash, and F.-Y. Porter, 1993: Diagnostic studies of two contrasting rainfall episodes in Hawaii: Dry 1981 and wet 1982. *J. Climate*, **6**, 1457–1462, doi:10.1175/1520-0442(1993)006<1457:DSOTCR>2.0.CO;2.

Collins, M., and Coauthors, 2010: The impact of global warming on the tropical Pacific Ocean and El Niño. *Nat. Geosci.*, **3**, 391–397, doi:10.1038/ngeo868.

——, and Coauthors, 2013: Long-term climate change: Projections, commitments and irreversibility. *Climate Change 2013: The Physical Science Basis*, T. F. Stocker et al., Eds., Cambridge University Press, 1029–1136.

Cram, R. S., and H. R. Tatum, 1979: Record torrential rainstorms on the island of Hawaii, January–February 1979. *Mon. Wea. Rev.*, **107**, 1653–1662, doi:10.1175/1520-0493(1979)107<1653:RTROTI>2.0.CO;2.

Cressman, G. P., 1959: An operational objective analysis system. *Mon. Wea. Rev.*, **87**, 367–374, doi:10.1175/1520-0493(1959)087<0367:AOOAS>2.0.CO;2.

Dee, D. P., and Coauthors, 2011: The ERA-Interim reanalysis: Configuration and performance of the data assimilation system. *Quart. J. Roy. Meteor. Soc.*, **137**, 553–597, doi:10.1002/qj.828.

Duffy, D. C., and F. Kraus, 2006: Science and the art of the solvable in Hawaii's extinction crisis. *Environ. Hawaii*, **16**, 3–6.

Elison Timm, O., and H. F. Diaz, 2009: Synoptic-statistical approach to regional downscaling of IPCC twenty-first-century climate projections: Seasonal rainfall over the Hawaiian Islands. *J. Climate*, **22**, 4261–4280, doi:10.1175/2009JCLI2833.1.

——, T. M. Takahashi, T. W. Giambelluca, and H. F. Diaz, 2013: On the relation between large-scale circulation pattern and heavy rain events over the Hawaiian Islands: Recent trends and future changes. *J. Geophys. Res. Atmos.*, **118**, 4129–4141, doi:10.1002/jgrd.50314.

——, T. W. Giambelluca, and H. F. Diaz, 2015: Statistical downscaling of rainfall changes in Hawai'i based on the CMIP5 global model projections. *J. Geophys. Res. Atmos.*, **120**, 92–112, doi:10.1002/2014JD022059.

Esteban, M. A., and Y. Chen, 2008: The impact of trade wind strength on precipitation over the windward side of the island of Hawaii. *Mon. Wea. Rev.*, **136**, 913–928, doi:10.1175/2007MWR2059.1.

Flato, G., and Coauthors, 2013: Evaluation of climate models. *Climate Change 2013: The Physical Science Basis*, T. F. Stocker et al., Eds., Cambridge University Press, 741–866.

Giambelluca, T. W., H. F. Diaz, and M. S. A. Luke, 2008: Secular temperature changes in Hawai'i. *Geophys. Res. Lett.*, **35**, L12702, doi:10.1029/2008GL034377.

——, Q. Chen, A. G. Frazier, J. P. Price, Y.-L. Chen, P.-S. Chu, J. K. Eischeid, and D. M. Delparte, 2013: Online rainfall atlas of Hawai'i. *Bull. Amer. Meteor. Soc.*, **94**, 313–316, doi:10.1175/BAMS-D-11-00228.1.

——, and Coauthors, 2014: Evapotranspiration of Hawai'i. U.S. Army Corps of Engineers Rep., 168 pp. [Available online at http://evapotranspiration.geography.hawaii.edu/assets/files/PDF/ET%20Project%20Final%20Report.pdf.]

Hara, M., T. Yoshikane, H. Kawase, and F. Kimura, 2008: Estimation of the impact of global warming on snow depth in Japan by the pseudo-global warming method. *Hydrol. Res. Lett.*, **2**, 61–64, doi:10.3178/hrl.2.61.

Held, I. M., and B. J. Soden, 2006: Robust responses of the hydrological cycle to global warming. *J. Climate*, **19**, 5686–5699, doi:10.1175/JCLI3990.1.

Hirota, N., and Y. N. Takayabu, 2013: Reproducibility of precipitation distribution over the tropical oceans in CMIP5 multi-climate models compared to CMIP3. *Climate Dyn.*, **41**, 2909–2920, doi:10.1007/s00382-013-1839-0.

IPCC, 2000: *Emissions Scenarios*. Cambridge University Press, 570 pp.

James, H. F., 1995: Prehistoric change to diversity and ecosystem dynamics on oceanic islands. *Biological Diversity and Ecosystem Function on Islands*, P. Vitousek, L. Loope, and H. Adsersen, Eds., Springer, 87–101.

Jokiel, P. L., and E. K. Brown, 2004: Global warming, regional trends and inshore environmental conditions influence coral bleaching in Hawaii. *Global Change Biol.*, **10**, 1627–1641, doi:10.1111/j.1365-2486.2004.00836.x.

Kane, H., C. H. Fletcher, L. N. Frazier, and M. M. Barbee, 2015: Critical elevation levels for flooding due to sea-level rise in Hawaii. *Reg. Environ. Change*, **15**, 1679–1687, doi:10.1007/s10113-014-0725-6.

Kawase, H., T. Yoshikane, M. Hara, F. Kimura, T. Yasunari, B. Ailikun, H. Ueda, and T. Inoue, 2009: Intermodel variability of future changes in the baiu rainband estimated by the pseudo global warming downscaling method. *J. Geophys. Res.*, **114**, D21110, doi:10.1029/2009JD011803.

Kharin, V. V., F. W. Zwiers, X. Zhang, and G. C. Hegerl, 2007: Changes in temperature and precipitation extremes in the IPCC ensemble of global coupled model simulations. *J. Climate*, **20**, 1419–1444, doi:10.1175/JCLI4066.1.

Kimura, F., and A. Kitoh, 2007: Downscaling by pseudo global warming method. ICCAP Final Rep., RIHN Project 1-1, 4 pp. [Available online at http://www.chikyu.ac.jp/P-C09/ICCAP/ICCAP_Final_Report/2/4-climate_kimura.pdf.]

King, C. W., 2014: A systems approach for investigating water, energy, and food scenarios in east-central Maui. The University of Texas at Austin Rep. to the Ulupono Initiative, Jackson School of Geosciences, 65 pp.

Knutson, T. R., J. J. Sirutus, S. T. Garner, G. A. Vecchi, and I. M. Held, 2008: Simulated reduction in Atlantic hurricane frequency under twenty-first-century warming conditions. *Nat. Geosci.*, **1**, 359–364, doi:10.1038/ngeo202.

Krushelnycky, P. D., L. L. Loope, T. W. Giambelluca, F. Starr, K. Starr, D. R. Drake, A. D. Taylor, and R. H. Robichaux, 2013: Climate associated population declines reverse recovery and threaten future of an iconic high elevation plant. *Global Change Biol.*, **19**, 911–922, doi:10.1111/gcb.12111.

Kuo, H. L., 1965: On formation and intensification of tropical cyclones through latent heat released by cumulus convection. *J. Atmos. Sci.*, **22**, 40–63, doi:10.1175/1520-0469(1965)022<0040:OFAIOT>2.0.CO;2.

——, 1974: Further studies of the parameterization of the influence of cumulus convection on large-scale flow. *J. Atmos. Sci.*, **31**, 1232–1240, doi:10.1175/1520-0469(1974)031<1232:FSOTPO>2.0.CO;2.

Lauer, A., and K. Hamilton, 2013: Simulating clouds with global climate models: A comparison of CMIP5 results with CMIP3 and satellite data. *J. Climate*, **26**, 3823–3845, doi:10.1175/JCLI-D-12-00451.1.

——, C. Zhang, O. Elison Timm, Y. Wang, and K. Hamilton, 2013: Downscaling of climate change in the Hawaii region using CMIP5 results: On the choice of the forcing fields. *J. Climate*, **26**, 10 006–10 030, doi:10.1175/JCLI-D-13-00126.1.

Leong, J.-A., and Coauthors, 2014: Hawai'i and U.S. affiliated Pacific islands. *Climate Change Impacts in the United States: The Third National Climate Assessment*, J. M. Melillo, T. C. Richmond, and G. W. Yohe, Eds., U.S. Global Change Research Program, 537–556, doi:10.7930/J0W66HPM.

Lyons, S. W., 1982: Empirical orthogonal function analysis of Hawaiian rainfall. *J. Appl. Meteor.*, **21**, 1713–1729, doi:10.1175/1520-0450(1982)021<1713:EOFAOH>2.0.CO;2.

McDonald, J. H., 2014: *Handbook of Biological Statistics.* 3rd ed. Sparky House Publishing, 299 pp.

Mearns, L., and Coauthors, 2012: The North American Regional Climate Change Assessment Program: Overview of phase I results. *Bull. Amer. Meteor. Soc.*, **93**, 1337–1362, doi:10.1175/BAMS-D-11-00223.1.

Norton, C., P.-S. Chu, and T. A. Schroeder, 2011: Estimating changes in future heavy rainfall events for Oahu, Hawaii: A statistical downscaling approach. *J. Geophys. Res.*, **116**, D17110, doi:10.1029/2011JD015641.

O'Gorman, P. A., and T. Schneider, 2009: The physical basis for increases in precipitation extremes in simulations of 21st-century climate change. *Proc. Natl. Acad. Sci. USA*, **106**, 14 773–14 777, doi:10.1073/pnas.0907610106.

Prein, A. F., and Coauthors, 2015: A review on regional convection-permitting climate modeling: Demonstrations, prospects, and challenges. *Rev. Geophys.*, **53**, 323–361, doi:10.1002/2014RG000475.

Qu, X., A. Hall, S. A. Klein, and P. M. Caldwell, 2015: The strength of the tropical inversion and its response to climate change in 18 CMIP5 models. *Climate Dyn.*, **45**, 375–396, doi:10.1007/s00382-014-2441-9.

Reynolds, R. W., T. M. Smith, C. Liu, D. B. Chelton, K. S. Casey, and M. G. Schlax, 2007: Daily high-resolution-blended analyses for sea surface temperature. *J. Climate*, **20**, 5473–5496, doi:10.1175/2007JCLI1824.1.

Rienecker, M. M., and Coauthors, 2011: MERRA: NASA's Modern-Era Retrospective Analysis for Research and Applications. *J. Climate*, **24**, 3624–3648, doi:10.1175/JCLI-D-11-00015.1.

Romine, B. M., C. H. Fletcher, M. M. Barbee, T. R. Anderson, and L. N. Frazer, 2013: Are beach erosion rates and sea-level rise related in Hawaii? *Global Planet. Change*, **108**, 149–157, doi:10.1016/j.gloplacha.2013.06.009.

Sakai, A. K., W. L. Wagner, and L. A. Merhoff, 2002: Patterns of endangerment in the Hawaiian flora. *Syst. Biol.*, **51**, 276–302, doi:10.1080/10635150252899770.

Sato, T., F. Kimura, and A. Kitoh, 2007: Projection of global warming onto regional precipitation over Mongolia using a regional climate model. *J. Hydrol.*, **333**, 144–154, doi:10.1016/j.jhydrol.2006.07.023.

Schroeder, T. A., 1993: Climate controls. *Prevailing Trade Winds: Weather and Climate in Hawaii*, M. Sanderson, Ed., University of Hawai'i Press, 12–36.

Stevenson, S., B. Fox-Kemper, M. Jochum, R. Neale, C. Deser, and G. Meehl, 2012: Will there be a significant change to El Niño in the twenty-first century? *J. Climate*, **25**, 2129–2145, doi:10.1175/JCLI-D-11-00252.1.

Tran, N., P. Illukpitiya, J. F. Yanagida, and R. Ogoshi, 2011: Optimizing biofuel production: An economic analysis for selected biofuel feedstock production in Hawaii. *Biomass Bioenergy*, **35**, 1756–1764, doi:10.1016/j.biombioe.2011.01.012.

Trauernicht, C., E. Pichett, C. P. Giardina, C. M. Litton, S. Cordell, and A. Beavers, 2015: The contemporary scale and context of wildfire in Hawaii. *Pac. Sci.*, **69**, 427–444, doi:10.2984/69.4.1.

Tu, C.-C., and Y.-L. Chen, 2011: Favorable conditions for the development of a heavy rainfall event over Oahu during the 2006 wet period. *Wea. Forecasting*, **26**, 280–300, doi:10.1175/2010WAF2222449.1.

Wang, G., D. Dommenget, and C. Frauen, 2015: An evaluation of the CMIP3 and CMIP5 simulations in their skill of simulating the spatial structure of SST variability. *Climate Dyn.*, **44**, 95–114, doi:10.1007/s00382-014-2154-0.

Wittenberg, A. T., 2009: Are historical records sufficient to constrain ENSO simulations? *Geophys. Res. Lett.*, **36**, L12702, doi:10.1029/2009GL038710.

Zhang, C., Y. Wang, A. Lauer, and K. Hamilton, 2012a: Configuration and evaluation of the WRF Model for the study of Hawaiian regional climate. *Mon. Wea. Rev.*, **140**, 3259–3277, doi:10.1175/MWR-D-11-00260.1.

——, ——, ——, ——, and F. Xie, 2012b: Cloud base and top heights in the Hawaiian region determined with satellite and ground-based measurements. *Geophys. Res. Lett.*, **39**, L15706, doi:10.1029/2012GL052355.

——, ——, K. Hamilton, and A. Lauer, 2016: Dynamical downscaling of the climate for the Hawaiian Islands. Part I: Present day. *J. Climate*, **29**, 3027–3048, doi:10.1175/JCLI-D-15-0432.1.

Zheng, Y., T. Shinoda, J.-L. Lin, and G. N. Kiladis, 2011: Sea surface temperature biases under the stratus cloud deck in the southeast Pacific Ocean in 19 IPCC AR4 coupled general circulation models. *J. Climate*, **24**, 4139–4164, doi:10.1175/2011JCLI4172.1.